

Parameters of V404 Cyg—A Black-Hole Binary

A. M. Cherepashchuk^{1,2}, N. V. Borisov³,
M. K. Abubekеров¹, D. K. Klochkov¹, and É. A. Antokhina²

¹Moscow State University, Vorob'evy gory, Moscow, 119899 Russia

²Sternberg Astronomical Institute, Universitetskii pr. 13, Moscow, 119899 Russia

³Special Astrophysical Observatory, Nizhniĭ Arkhyz, Russia

Received March 15, 2004; in final form, May 27, 2004

Abstract—We present the results of spectroscopic observations of the X-ray binary V404 Cyg obtained on the 6-m telescope of the Special Astrophysical Observatory in 2001–2002. We have used a statistical approach to interpret the radial-velocity curve of V404 Cyg. We derived the dependence of the mass of the X-ray emitting component m_x on the mass of the optical component m_v via an analysis of the radial-velocity curve based on profiles of the CaI 6439.075 Å absorption line synthesized in a Roche model. Using the orbital inclination estimated from the ellipticity of the optical component, $i = 54^\circ\text{--}64^\circ$, and the component-mass ratio $q = m_x/m_v = 16.7$ found from the rotational broadening of the spectral lines, we obtain $m_x = 10.65 \pm 1.95 M_\odot$ for the mass of the black hole. © 2004 MAIK “Nauka/Interperiodica”.

1. INTRODUCTION

The X-ray nova GS 2023+338 was first discovered by the Ginga space probe during an outburst on May 22, 1989 [1]. This discovery was subsequently confirmed by Sunyaev *et al.* [2]. During the outburst, the magnitude of GS 2023+338 changed from $V \sim 18.3^m$ to $V = 11.6^m$. Soon afterward, an optical counterpart to the X-ray source was identified: V404 Cyg, which had been classified as a nova after an outburst in 1938 [3, 4].

The X-ray nova V404 Cyg contains a K0IV optical subgiant that fills its Roche lobe and a black hole that accretes matter from an accretion disk. The mass function of the optical star in V404 Cyg is $f_v = 6.08 \pm 0.06 M_\odot$ [5]; this is much higher than the limiting mass for neutron stars, providing evidence that the compact component in the system is a black hole. The absence of X-ray pulsations from the compact object prevents the direct determination of the mass of the optical component. Estimates of the mass of the optical star based on its spectral type vary from $0.5 M_\odot$ to $1.0 M_\odot$ [6].

Current estimates of the parameters of the X-ray source are not very accurate. Based on the I light curve, the range of possible orbital inclinations was determined to be $46^\circ\text{--}73^\circ$ and the component-mass ratio to be $q = m_x/m_v = 8\text{--}12$ [7]. The measured semi-amplitude of the radial velocity variations, $K_v = 211 \pm 4$ km/s, yields for the mass function of the optical star $f_v = 6.3 \pm 0.3 M_\odot$. Assuming that the mass of the subgiant is close to $1.0 M_\odot$, Wagner

et al. [7] concluded that the mass of the compact object is $8\text{--}12 M_\odot$.

A more accurate semi-amplitude for the radial velocity of the optical star was found in [5]: $K_v = 208.5 \pm 0.7$ km/s; this corresponds to the mass function $f_v = 6.08 \pm 0.06 M_\odot$ quoted above. The component-mass ratio $q = 16.7 \pm 1.3$ was estimated from the rotational broadening of lines of metals at $6400\text{--}6600$ Å. Assuming that the highest possible orbital inclination is 80° (as follows from the absence of X-ray eclipses [8]) and that the mass of the optical star is $0.2\text{--}1.3 M_\odot$, we obtain for the mass of the compact object $7\text{--}24 M_\odot$.

Analysis of the K light curve of V404 Cyg yields the orbital inclination $i = 52^\circ\text{--}60^\circ$ [6]. Using the component-mass ratio $q = 16.7$ [5] and the mass of the optical component $0.5\text{--}1.0 M_\odot$, we find for the mass of the compact object $10\text{--}15 M_\odot$.

Analysis of the H light curve of V404 Cyg yields $i = 59^\circ\text{--}73^\circ$ [9]. For this range of inclinations, the mass of the black hole does not exceed $12.5 M_\odot$. For the component-mass ratio $q = 16.7$, the mass of the black hole is close to $9.5 M_\odot$.

The R light curve combined with the spectroscopic component-mass ratio $q = 16.7$ [5] gives $i = 56^\circ \pm 2^\circ$ [10]; variability of the light curve on a time scale of six hours was reported in this same paper. Six-hour variability of the H α profile is also observed, but the brightness and H α variations of the system are not correlated [11, 12]. Hynes *et al.* [13] describe the growth and decline of the equivalent width and

Table 1. Spectroscopic observations of V404 Cyg

Date	UT	Exposure, s	Number of spectra	Spectral interval, Å	Resolution, Å
July 12, 2001	18:07–20:30	2700	3	5700–8200	5.5
July 14, 2001	18:52–20:26	2700	2	5700–8200	5.5
July 15, 2001	20:20–21:53	2700	2	5700–8200	5.5
July 16, 2001	21:09–22:40	2700	2	5700–8200	5.5
June 14, 2002	17:35–20:14	1800	5	5500–6800	3.0
July 9, 2002	18:25–19:35	1800	2	5500–6800	3.0
July 10, 2002	18:43–20:20	1800	3	5500–6800	3.0
July 11, 2002	16:52–20:02	1800	6	5500–6800	3.0
July 12, 2002	18:56–19:57	1800	2	5500–6800	3.0

variations of the H α emission profile on time scales down to ~ 1 –2 h. Pavlenko *et al.* [10] include fluctuations of the photoionizing flux from the compact object due to local flares in the accretion disk or the disk corona among possible origins for the variation of the H α emission equivalent width [13], however, the mechanism underlying the fast variations of the H α equivalent width is not known with certainty. The asymmetry of the H α emission wings likewise remains poorly understood (for more details see [13]).

Our aim was to more accurately determine the radial-velocity curve of the X-ray nova V404 Cyg and

Table 2. Observed barycentric radial velocities of V404 Cyg (adopted zero Julian epoch is $JD_0 = 2448813.873$ [5])

Phase	Radial velocity, km/s
0.229	187.10
0.295	195.90
0.365	161.20
0.387	139.80
0.535	–58.39
0.606	–111.09
0.696	–198.10
0.770	–212.50
0.930	–68.42

the parameters of the close binary system, as well as study the short-time-scale variability of the H α emission profile.

2. OBSERVATIONAL DATA

Two sets of spectroscopic observations of V404 Cyg were obtained using the 6-m telescope of the Special Astrophysical Observatory between July 12 and 16, 2001 and between June 11 and July 12, 2002. The observations were carried out at the primary focus using a UAGS high-power, long-slit spectrograph and a PM1024 CCD with 1024×1024 pixels and a pixel size of $24 \times 24 \mu\text{m}$. In 2001, we used a diffraction grating with a dispersion of 651 lines/mm, yielding an inverse linear dispersion of $3.1 \text{ \AA}/\text{pixel}$ in the spectral interval studied, 5700–8200 Å. The resolution of the resulting spectrograms was 5.5 Å.

In 2002, we used a R1305/17 diffraction grating with a dispersion of 1305 lines/mm, providing an inverse linear dispersion of $1.5 \text{ \AA}/\text{pixel}$ and a resolution of 3.0 \AA at 5500–6800 Å. A log of the observations is given in Table 1.

All the spectra were calibrated against a HeNe light source. The spectra were reduced using the MIDAS package, including standard flat fielding, background subtraction, bias correction, and elimination of “hot” pixels. The single white dwarf BD+284211 was used as a spectrophotometric standard for all the spectrograms. The KOIV star HR8857 [5] was used as a radial-velocity standard.

The radial velocities of V404 Cyg were derived from the shift of blends at 6400–6520 Å relative to the

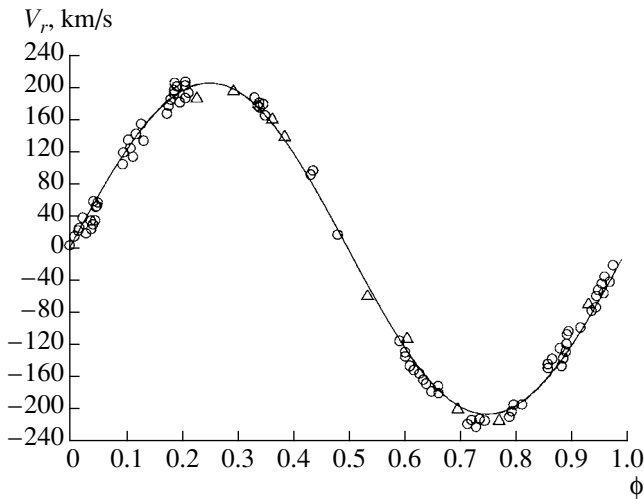


Fig. 1. Folded observed radial-velocity curve of the optical component of V404 Cyg. The open circles show the observed radial velocities derived by Casares and Charles [5] from absorption lines of metals, while the open triangles show the radial velocities found in the present study. The solid curve is the theoretical radial velocity curve for the Roche model based on the synthesized CaI 6439.075 Å absorption line profile assuming $m_x = 10.46 M_\odot$, $m_v = 0.7 M_\odot$, and $i = 59^\circ$ (the remaining parameters are listed in Table 3); no correction for the response function has been made. The dashed curve shows the theoretical radial-velocity curve for a point-mass model with $m_x = 10.46 M_\odot$, $m_v = 0.7 M_\odot$, and $i = 59^\circ$. This latter curve nearly coincides with the curve for the Roche model.

blends in the same wavelength interval of the radial-velocity standard HR 8857. Table 2 gives the observed radial velocities of the optical component of V404 Cyg corrected for the Earth’s motion and the systemic velocity.

We constructed the folded radial-velocity curve using our spectroscopic data along with the radial velocities from [5], which were derived from the shift for the wavelength interval 6212–6605 Å relative to this same interval in the spectrum of the radial-velocity standard, HR 8857. The folded curve enabled us to determine the orbital period of the V404 Cyg binary more precisely. We adopted $JD_0 = 2448813.873$ for the zero Julian epoch [5]. The new orbital period, $P_{orb} = 6^d4715 \pm 0.0001$, agrees with the old value, $P_{orb} = 6^d4714 \pm 0.0001$ [5], within the errors.

The folded observed radial-velocity curve based on our spectroscopic data and the data of [5] is shown in Fig. 1. The radial velocities were averaged over phase intervals to reduce the influence of random errors (Fig. 2). Since the observed radial velocities are not distributed in phase very uniformly, the rms deviation of the mean radial velocity at phase 0.508

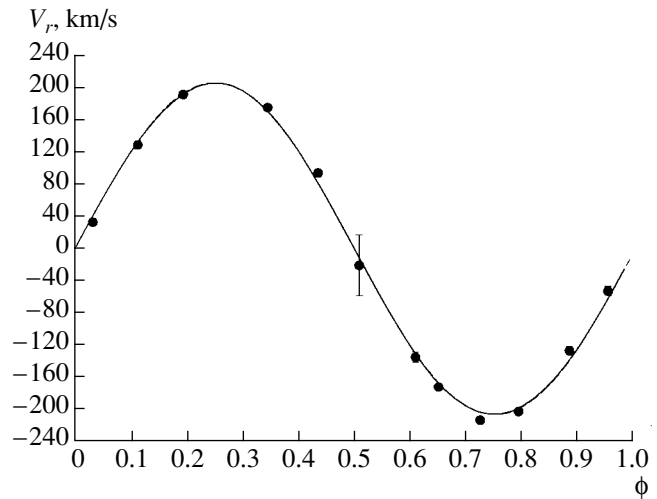


Fig. 2. Radial velocities averaged over phase intervals (filled circles). For comparison, theoretical radial-velocity curves for the Roche model (solid) and point-mass model (dashed) for the case $m_x = 10.46 M_\odot$, $m_v = 0.7 M_\odot$, and $i = 59^\circ$ are shown.

is 37.80 km/s (or 18.1% of the radial-velocity semi-amplitude). This large rms deviation is due to the large gradient of the regular radial-velocity variations near phase 0.5. Since the rms deviation of the observed radial velocity σ_{V_r} at phase 0.508 is much larger than in other phase intervals (where it is $\sim 2\text{--}3\%$ of the radial-velocity semi-amplitude; Fig. 2), and thus gives rise to an appreciable “perturbation” of the residuals [see (1) below], we excluded the mean observed radial velocity at phase 0.508 when fitting the mean radial-velocity curve.

3. FITTING OF THE MEAN RADIAL-VELOCITY CURVE

The optical component of V404 Cyg fills its inner Roche lobe. The tidal action of the relativistic companion makes the shape of the optical star non-spherical. The side of the optical component facing the relativistic object is heated by the incident X-ray emission. Therefore, we fit the mean radial velocities using a Roche model that is able to take into account this interaction between the components to some extent. The parameters of the Roche model for the X-ray binary V404 Cyg are given in Table 3.

The presence of observable X-ray emission from the V404 Cyg binary provides evidence that the KOIV optical star fills its Roche lobe. Since this star fills its Roche lobe over a time determined by its nuclear evolution time scale, which is $\sim 10^{10}$ yr, the orbit of the close binary has enough time to circularize, and the rotation of the optical component becomes

Table 3. Numerical input parameters for the synthesis of the radial-velocity curves of the optical component of V404 Cyg in the Roche model

P , day	6.4715	Period
e	0.0	Eccentricity
i , deg	54, 59, 64	Orbital inclination
μ	1.0	Roche lobe filling factor for optical component
f	1.0	Ratio of the rotational velocity of the optical star to the synchronous rotational velocity
T_{eff} , K	5500	Effective temperature of the optical component
β	0.08	Gravitational darkening coefficient
k_x	0.03	Ratio of the X-ray luminosity of the relativistic component and bolometric luminosity of the optical component, L_x/L_v
A	1.0	Coefficient of reprocessing of incident X-ray radiation
u	0.5	Limb-darkening coefficient

synchronous with the orbital motion. Therefore, our calculations assume that the orbit of V404 Cyg is circular and the ratio of the spin and orbital rotational velocities is $f = 1.0$.

We consider the masses of both components and the orbital inclination of V404 Cyg to be unknown parameters. We found the solution via a step-by-step search through the parameter values considered. We obtained a set of masses for the compact object m_x for masses of the optical component m_v of $0.5 M_\odot$, $0.7 M_\odot$, and $0.9 M_\odot$ and orbital inclinations i of 54° , 59° , and 64° . This yields the dependence of the mass of the compact object on the mass of the optical component and orbital inclination. The orbital inclinations were selected based on earlier fitting of the R , K , and H light curves of the close binary, which gave the estimates $56^\circ \pm 2^\circ$ [10], $56^\circ \pm 4^\circ$ [6], and $59^\circ - 73^\circ$ [9], respectively. The statistical adequacy of the model was tested at the $\alpha = 5\%$ significant level.

Since the radial velocity of the optical component was determined from absorption lines of metals at $6200\text{--}6500 \text{ \AA}$ both in the present study and in [5], our theoretical radial velocities are based on synthesized profiles of the CaI 6439.075 \AA absorption line. Since absorption lines of metals in the spectrum of the optical component of V404 Cyg have small widths ($\sim 1 \text{ \AA}$), the theoretical radial-velocity curves were computed from the CaI 6439.075 \AA profile convolved with a Gaussian instrumental profile with a full width at the half maximum of $\text{FWHM} = 0.5 \text{ \AA}$. This FWHM was adopted because most of the radial velocities included in the folded curve (Fig. 2) were

derived from spectra obtained with an instrumental $\text{FWHM} = 0.5 \text{ \AA}$ [5]. For comparison purposes, we also fit the observed mean radial-velocity curve of V404 Cyg using synthesized CaI 6439.075 \AA profiles without convolving with a response function. Figure 3 shows the synthesized CaI 6439.075 \AA absorption profiles at orbital phases of 0.00 and 0.25 for both cases.

The residual differences between the mean observed and theoretical radial-velocity curves were computed as

$$\Delta(m_x) = \frac{\sum_{j=1}^M (n_j - 1) \sum_{j=1}^M n_j (V_j^{\text{teor}} - \bar{V}_j^{\text{obs}})^2}{M \sum_{j=1}^M n_j (n_j - 1) \sigma_j^2}, \quad (1)$$

where \bar{V}_j^{obs} is the observed radial velocity averaged over a phase interval centered at $\bar{\phi}_j$, V_j^{teor} is the theoretical radial velocity at the same phase, σ_j is the rms deviation of \bar{V}_j^{obs} from the observed radial velocity in the phase interval with its center at $\bar{\phi}_j$, M is the number of phase intervals, and n_j is the number of individual averaged observations in phase interval j .

The value of $\Delta(m_x)$ is distributed according to a Fisher law $F_{M, \sum_{j=1}^M (n_j - 1), \alpha}$ [14]. We can find the set of acceptable values for m_x for a given significance level α and a specified value of m_v . This set contains

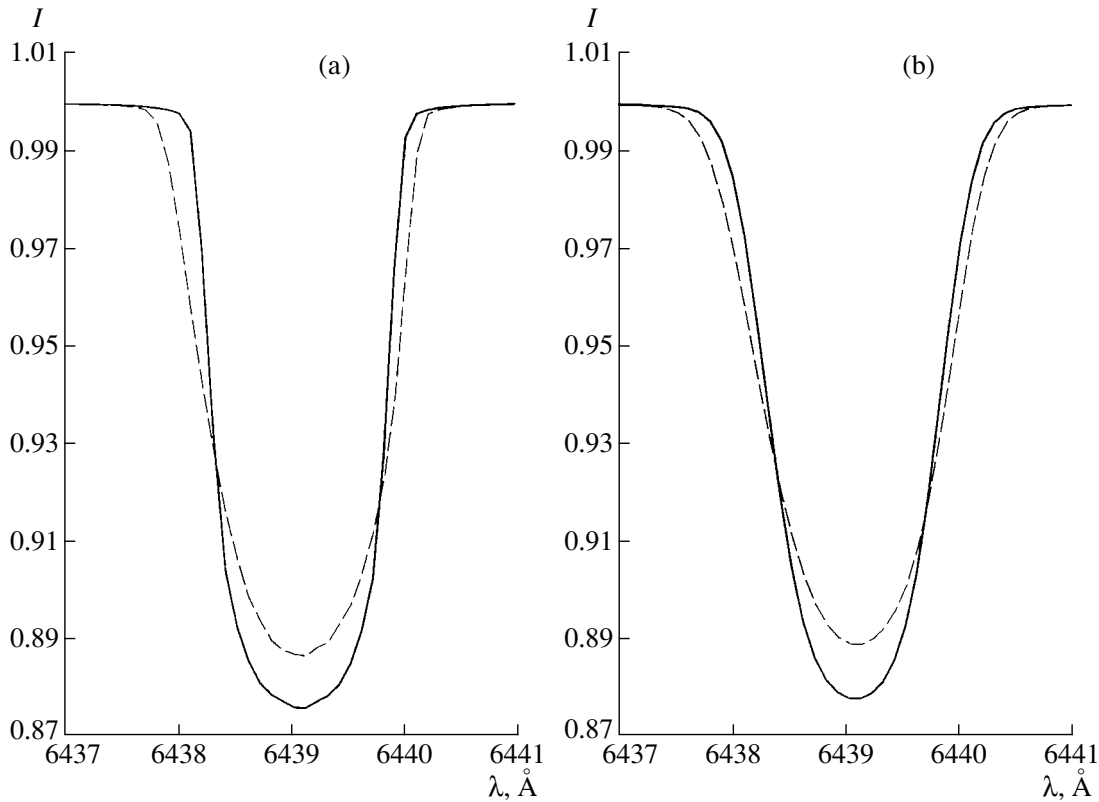


Fig. 3. (a) Synthetic profiles of the CaI 6439.075 Å absorption line calculated in the Roche model for $m_x = 10.46 M_\odot$, $m_v = 0.7 M_\odot$, and $i = 59^\circ$ (for the remaining parameters see Table 3) at orbital phases 0.00 (solid) and 0.25 (dashed). (b) The same profiles convolved with a Gaussian response function with FWHM = 0.5 Å. The profiles at orbital phase 0.25 are corrected for the Doppler shift.

values of m_x obeying the condition

$$\Delta(m_x) \leq F_{M, \sum_{j=1}^M (n_j - 1), \alpha}$$

The algorithm used to compute the theoretical absorption-line profiles and theoretical radial-velocity curves is described in [15, 16], and we do not present it here. Note, however, that computing the local shape of the CaI 6439.075 Å absorption profile using this algorithm requires the solution of the radiative-transfer equation for each area element. This differs from the algorithm for synthesizing radial-velocity curves from the H γ absorption profile applied in [17], which included computation of the local shape of the profile from an area element via the interpolation of tabulated values of this profile given by Kurucz [18].

The residuals found by fitting the mean observed radial-velocity curve are shown in Fig. 4; this figure shows that it is important to take into account the instrumental profile. The theoretical radial-velocity curves computed without including the effect of the response function on the synthesized CaI 6439.075 Å

absorption profile are not in agreement with the observed data: the close-binary models are rejected at the $\alpha = 5\%$ significance level (Fig. 4b).

Table 4 presents the relation between the component masses for various orbital inclinations derived in the Roche model based on the synthesized CaI 6439.075 Å profiles convolved with the response function. The same relation without this convolution is presented in Table 5. The results are shown in graphical form in Fig. 5. Since the residual differences between the theoretical and observed radial-velocity curves are unacceptably large at the $\alpha = 5\%$ significance level when the response function is not taken into account, the confidence intervals for the mass of the compact object are omitted in Table 5 and Fig. 5b.

4. DEPENDENCE OF THE SHAPE OF THE RADIAL-VELOCITY CURVE OF V404 Cyg ON ORBITAL INCLINATION

We carried out special calculations of the theoretical radial-velocity curves in the Roche model to study the dependence of the shape of the radial-velocity curve on the orbital inclination of V404 Cyg. The

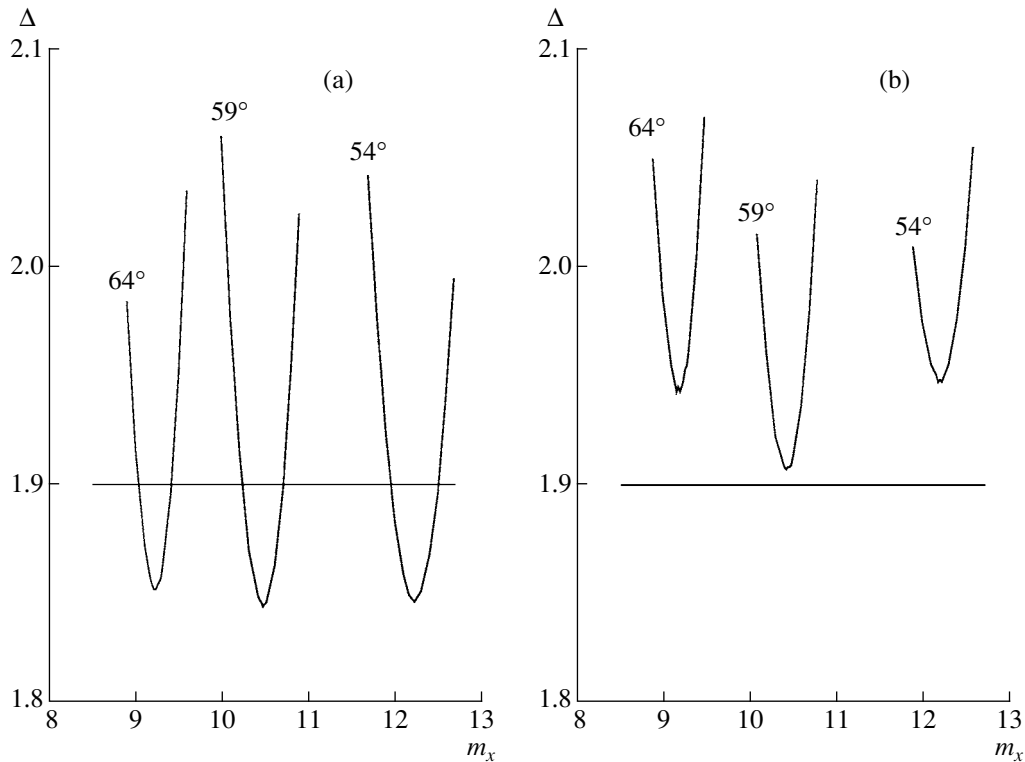


Fig. 4. (a) Residuals for the fitting of the radial-velocity curve derived in the Roche model for $m_v = 0.7 M_\odot$ and orbital inclinations $i = 54^\circ$, 59° , and 64° (for the remaining parameters see Table 3). The curve is based on the synthesized CaI 6439.075 Å profile and includes the effect of a response function with FWHM = 0.5 Å. (b) Same as (a) but without the effect of the response function.

mass of the optical star was taken to be $m_v = 0.7 M_\odot$, and the mass of the black hole to be $m_x = 10 M_\odot$. Calculations were carried out for inclinations $i = 40^\circ$, 54° , 64° , and 80° , with the remaining parameters of the Roche model unchanged (see Table 3). Since the radial-velocity semiamplitude K_v increases with the orbital inclination, the computed theoretical radial velocity curves were normalized to the maximum radial velocity in the phase interval 0.0–0.5. The difference in the shapes of the radial-velocity curves is maximum at phase $\phi = 0.36$. The difference of the radial-velocity curves for $i = 40^\circ$ and $i = 80^\circ$ was $\sim 0.3\%$ of the semiamplitude K_v when the response function was taken into account when computing the synthesized CaI 6439.075 Å profiles and $\sim 0.5\%$ when the response function was not taken into account. For comparison, the difference in the shape of the radial-velocity curves for close binaries with parameters similar to that of Cyg X-1 ($q = m_x/m_v \simeq 0.5$) was $\sim 3\%$ of K_v when the orbital inclination was varied from $i = 40^\circ$ to $i = 80^\circ$ [19].

In the case of the X-ray nova V404 Cyg, increasing the orbital inclination from $i = 54^\circ$ to $i = 64^\circ$ resulted in variations of the shape of the radial-velocity curve of the semiamplitude K_v by $\sim 0.10\%$ or

$\sim 0.13\%$ when the CaI 6439.075 Å profile was or was not convolved with the response function. Because the shape of the radial-velocity curve varies little with such variations of the orbital inclination, the residual minima for the different inclinations do not differ as much as in the case of Cyg X-1 [19, Fig. 5] (Fig. 4).

The rms error σ_{V_r} of the observed mean radial-velocity curve of V404 Cyg is $\sim (2\text{--}3)\%$ of its semiamplitude K_v , preventing estimation of the orbital inclination as was done for Cyg X-1 [19]. However, the Roche model can be used to estimate the orbital inclination from the radial-velocity curve, since the minimum residuals are different for different inclinations (Fig. 4). This is especially clearly visible in Fig. 4b. For successful estimation of the orbital inclination of V404 Cyg from the radial-velocity curve, σ_{V_r} must be $\sim 0.10\%$ of K_v or, in absolute units, ~ 0.2 km/s. Therefore, further high-quality spectroscopic observations of V404 Cyg are promising for this purpose.

5. COMPONENT MASSES IN V404 Cyg

The component-mass ratio $q = m_x/m_v$ found from the rotational broadening of metal lines in the spectrum of the optical component of V404 Cyg is 16.7 [5]. By drawing the corresponding line in the

Table 4. Dependence of the m_x on m_v in the Roche model. The effect of the response function on the synthesized CaI 6439.075 Å profile is taken into account

m_v, M_\odot	m_x, M_\odot		
	$i = 54^\circ$	$i = 59^\circ$	$i = 64^\circ$
0.5	$11.87^{+0.24}_{-0.22}$	$10.13^{+0.21}_{-0.23}$	$8.87^{+0.22}_{-0.19}$
0.7	$12.22^{+0.30}_{-0.27}$	$10.46^{+0.25}_{-0.23}$	$9.21^{+0.21}_{-0.18}$
0.9	$12.56^{+0.28}_{-0.27}$	$10.78^{+0.26}_{-0.25}$	$9.53^{+0.20}_{-0.19}$

plot showing the relation between the component masses (Fig. 5), we find that, for $i = 54^\circ - 64^\circ$, the masses of the black hole and optical star are $m_x = 8.7 - 12.6 M_\odot$ and $m_v = 0.52 - 0.76 M_\odot$. Thus, the mean mass of the black hole in V404 Cyg is $10.65 \pm 1.95 M_\odot$.

6. VARIABILITY OF THE H α EMISSION PROFILE

Casares *et al.* [11] were the first to point out the S-wave variability of the H α emission profile; they estimated the period of this variability to be 5.7 h. Later, the more accurate period of 5.656 h was found from a larger number of spectrophotometric observations obtained in 1990–1991 [12].

The most detailed study of the short-time optical variability and behavior of the H α line in V404 Cyg was carried out by Hynes *et al.* [13], who found a qualitative correlation between the behavior of the continuum and the H α equivalent width. An increase of the continuum is observed with increase in the H α equivalent width. Both the continuum from the accretion disk and the H α flux vary by more than a factor of two over one to two hours.

During the nights of June 14 and July 11, 2002, we obtained five and six spectra at 5500–6800 Å (Table 1), enabling us to study the behavior of the H α line on time scales ~ 30 min. The H α emission profiles are shown in Fig. 6, and the profiles averaged over a night are shown in Fig. 7. We determined the mean profile by taking the arithmetic mean of all H α profiles obtained during a night. Figures 6 and 7 show that the emission profile not only experiences significant variations during the course of a night, but also varies strongly from night to night.

We investigated the short-term variability of the H α emission profile. We estimated the deviation of a given H α profile from the profile averaged over the night using the Fisher statistical criterion, averaging the relative intensities of the H α emission lines over

Table 5. Dependence of m_x on m_v in the Roche model. The effect of the response function on the synthesized CaI 6439.075 Å profile has not been included

m_v, M_\odot	m_x, M_\odot		
	$i = 54^\circ$	$i = 59^\circ$	$i = 64^\circ$
0.5	11.83	10.10	8.86
0.7	12.20	10.42	9.18
0.9	12.54	10.77	9.48

wavelength intervals of ~ 5 Å. The residuals were computed as

$$\Delta(I^{obs}(t)) = \frac{\sum_{j=1}^M (n_j - 1)}{M} \quad (2)$$

$$\times \frac{\sum_{j=1}^M n_j (I_j^{mean} - \bar{I}_j^{obs}(t))^2}{\sum_{j=1}^M n_j (n_j - 1) \sigma_j^2},$$

where \bar{I}_j^{obs} is the observed mean relative intensity of the H α line in the wavelength interval centered at $\bar{\lambda}_j$ at time t , I_j^{mean} is the mean relative intensity of the averaged H α line profile in the wavelength interval centered at $\bar{\lambda}_j$ at time t , σ_j is the rms deviation of $\bar{I}_j^{obs}(t)$ in a given wavelength interval centered at $\bar{\lambda}_j$, M is the average number of wavelength intervals, and n_j the number of averaged relative intensities in the wavelength interval j .

We found the times t when the H α profile deviated significantly from the nightly averaged profile for a specified significance level α . The deviation of a profile from the mean profile was considered to be significant if

$$\Delta(I^{obs}(t)) \geq F_{M, \sum_{j=1}^M (n_j - 1), \alpha}.$$

We considered the $\alpha = 5\%$ significance level for our analysis. The results are presented in Fig. 8, which shows that significant deviations from the mean level occurred on a time scale of about two hours on the night of June 14, 2002, and on a time scale of $\sim 0.5 - 1$ h on the night of July 11, 2002. The behavior of the line is striking. A phase of intense growth of the emission line component can suddenly change into a decrease, and vice versa. The change of phases may occur in ~ 0.5 h (Figs. 6b and 8b).

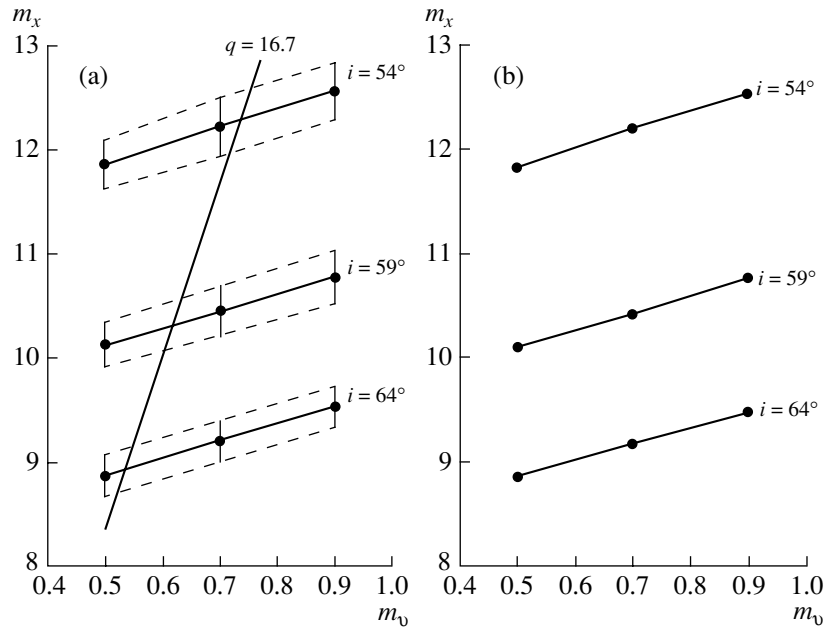


Fig. 5. (a) Relation between the masses of the compact object and optical star in V404 Cyg derived via analysis of the mean radial-velocity curve in the Roche model based on the CaI 6439.075 Å profile and convolved with a Gaussian response function with FWHM = 0.5 Å. The straight line corresponds to the component-mass ratio $q = m_x/m_o = 16.7$ [5]. (b) Same as (a) without including the effect of the response function.

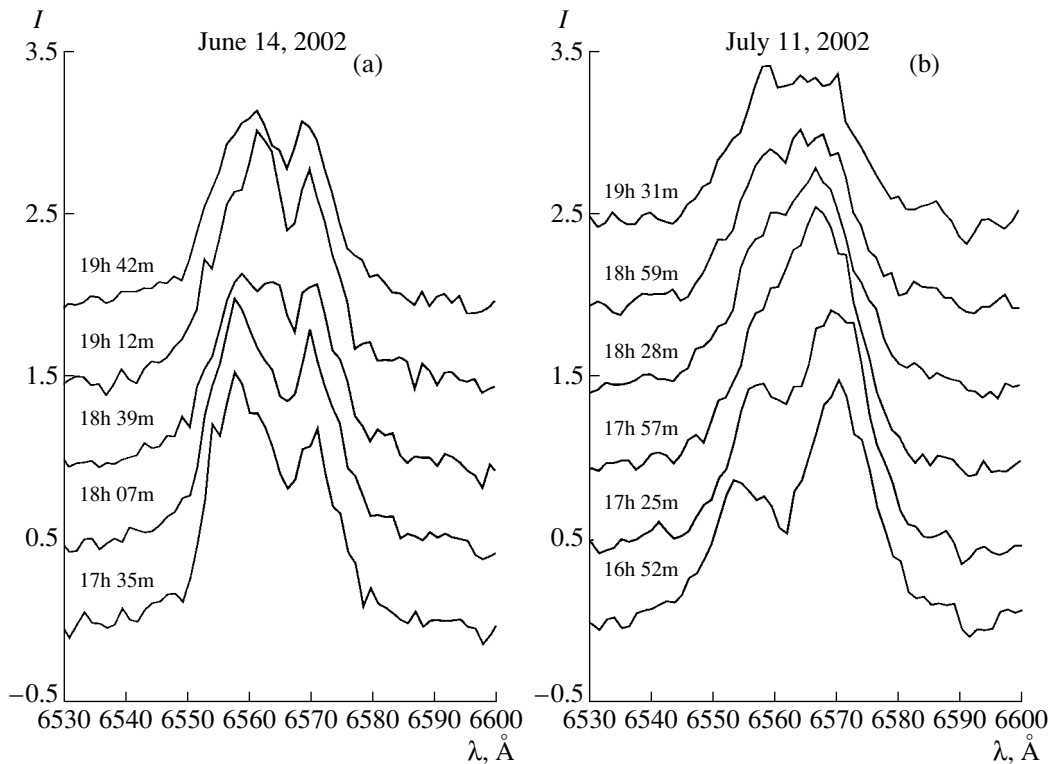


Fig. 6. H α emission profiles obtained on (a) June 14, 2002 at orbital phase $\phi = 0.365$ and (b) July 11, 2002 at orbital phase $\phi = 0.535$. For ease of viewing, the profiles have been shifted vertically relative to one another.

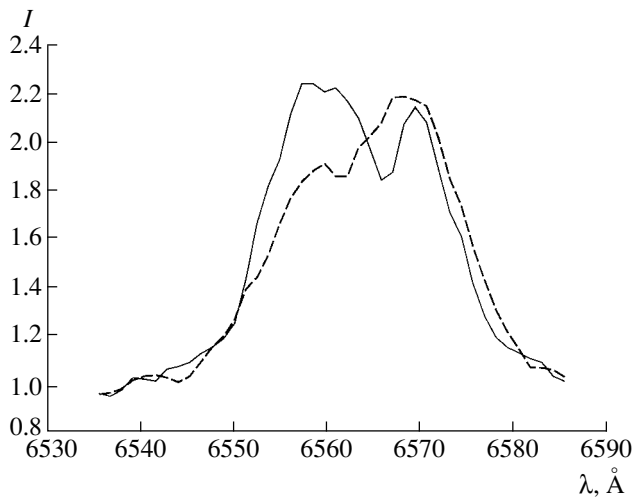


Fig. 7. Mean H α emission profiles obtained during the nights of June 14, 2002 at orbital phase $\phi = 0.365$ (solid) and July 11, 2002 at orbital phase $\phi = 0.535$ (dashed).

The origin of the H α variability has not been established. Proposed sources of the S-wave variability include the motion of a hot spot in the accretion disk [12], chromospheric activity of the optical component, and reconnection of magnetic field lines in the accretion disk [13]. No unique mechanism for the S-wave short-time-scale variability of the H α emission in V404 Cyg is known. Correct interpretation of the data requires a long series of observations with high time resolution, and studies in this direction should be continued.

7. CONCLUSION

The main result of our study is our derivation of the relation between the masses of the two components in the X-ray nova V404 Cyg in a Roche model for orbital inclinations $i = 54^\circ$ – 64° . Combined with the spectroscopically determined component-mass ratio $q = 16.7$ [5], these dependences yield $m_x = 10.65 \pm 1.95 M_\odot$ for the mass of the black hole and $m_v = 0.64 \pm 0.12 M_\odot$ for the mass of the optical star.

It is not currently possible to constrain the orbital inclination of V404 Cyg using the observed mean radial-velocity curve. The accuracy required for this is $\sim 0.10\%$ of the radial-velocity semi-amplitude K_v , while the accuracy of the observed mean radial-velocity curve is $\sim (2-3)\%$ of K_v . Thus, the averaged effects of the orbital variability of the absorption-line profiles contributing to the radial-velocity curves of low-mass X-ray binary systems ($q \gg 1$) influence the shape of the line relatively weakly. Therefore, the orbital inclinations of low-mass X-ray binary systems must be determined directly from the orbital variability of absorption-line profiles [20, 21]. This requires

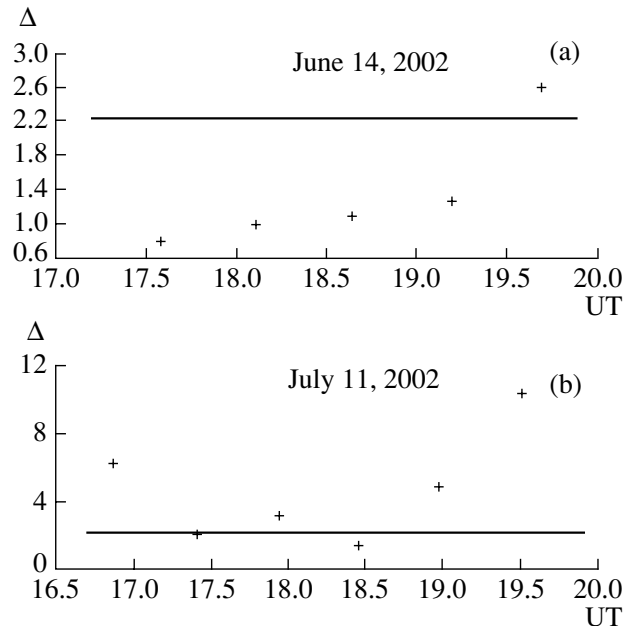


Fig. 8. Deviations of the H α emission profile from the nightly averaged profile on (a) June 14, 2002 at orbital phase $\phi = 0.365$ and (b) July 11, 2002 at orbital phase $\phi = 0.535$. The straight lines show critical levels of the residuals for the Fisher criterion for the $\alpha = 5\%$ significance level.

high-quality spectra of V404 Cyg with resolution $R \simeq 50\,000$ on the largest 8–10 m new-generation telescopes.

We also determined the typical time scales for variability of the H α emission profile. Significant variations of the profile shape and equivalent width occur on time scales of ~ 0.5 – 2 h. The origin of variability of the photoionizing flux has not been established [13], and studies of this problem require further spectroscopic observations of V404 Cyg.

ACKNOWLEDGMENTS

This work was supported by Russian Foundation for Basic Research (project no. 02-02-17524) and a grant from the program “Leading Scientific Schools of Russia” (NSh 388.2003.2).

REFERENCES

1. F. Makino *et al.*, IAU Circ., No. 4782 (1989).
2. R. Sunyaev *et al.*, IAU Circ., No. 4800 (1989).
3. B. G. Marsden, IAU Circ., No. 4783 (1989).
4. R. M. Wagner, T. J. Kreidl, S. B. Howell, *et al.*, IAU Circ., No. 4797 (1989).
5. J. Casares and P. A. Charles, Mon. Not. R. Astron. Soc. **271**, L5 (1994).
6. T. Shahbaz, F. A. Ringwald, J. C. Bunn, *et al.*, Mon. Not. R. Astron. Soc. **271**, L10 (1994).

7. M. R. Wagner, T. J. Kreidl, S. B. Howell, and S. G. Starrfield, *Astrophys. J.* **401**, L97 (1992).
8. Y. Tanaka, in *Proceedings of the 23rd ESLAB Symposium on Two Topics in X-Ray Astronomy*, Ed. by H. J. Battrick (ESA Publ. Div., SP-296, 1989), p. 1.
9. D. Sanwal, E. L. Robinson, E. Zhang, *et al.*, *Astrophys. J.* **460**, 437 (1996).
10. E. P. Pavlenko, A. C. Martin, J. Casares, *et al.*, *Mon. Not. R. Astron. Soc.* **281**, 1094 (1996).
11. J. Casares, P. A. Charles, T. Naylor, and E. P. Pavlenko, *Mon. Not. R. Astron. Soc.* **265**, 834 (1993).
12. J. Casares and P. A. Charles, *Mon. Not. R. Astron. Soc.* **255**, 7 (1992).
13. R. I. Hynes, C. Zurita, C. A. Haswell, *et al.*, *Mon. Not. R. Astron. Soc.* **330**, 1009 (2002).
14. D. Hudson, *Statistics. Lectures on Elementary Statistics and Probability* (Geneva, 1964; Mir, Moscow, 1970).
15. É. A. Antokhina, A. M. Cherepashchuk, and V. V. Shimanskiĭ, *Izv. Ross. Akad. Nauk, Ser. Fiz.* **67**, 293 (2003).
16. É. A. Antokhina, A. M. Cherepashchuk, and V. V. Shimanskiĭ, *Astron. Zh.* **81** (2004, in press).
17. É. A. Antokhina and A. M. Cherepashchuk, *Astron. Zh.* **71**, 420 (1994) [*Astron. Rep.* **38**, 367 (1994)].
18. R. L. Kurucz, *Astrophys. J., Suppl. Ser.* **40**, 1 (1979).
19. M. K. Abubekero, E. A. Antokhina, and A. M. Cherepashchuk, *Astron. Zh.* **81**, 606 (2004).
20. É. A. Antokhina and A. M. Cherepashchuk, *Pis'ma Astron. Zh.* **23**, 889 (1997) [*Astron. Lett.* **23**, 773 (1997)].
21. T. Shahbaz, *Mon. Not. R. Astron. Soc.* **298**, 153 (1998).

Translated by L. Yungel'son